

Origin of the Very High Energy γ -rays in the Low-luminosity Active Galactic Nucleus NGC 4278

Ji-Shun Lian,¹ Jia-Xuan Li,¹ Xin-Ke Hu,² Ying-Ying Gan,¹ Tan-Zheng Wu,¹ and Jin Zhang^{†1}

¹*School of Physics, Beijing Institute of Technology, Beijing 100081, People's Republic of China; j.zhang@bit.edu.cn*

²*Guangxi Key Laboratory for Relativistic Astrophysics, School of Physical Science and Technology, Guangxi University, Nanning 530004, People's Republic of China*

ABSTRACT

NGC 4278, a Low-luminosity active galactic nucleus (AGN), is generally classified as a low-ionization nuclear emission line region (LINER) type AGN. Recently, it is reported to be associated with a very high energy (VHE) γ -ray source 1LHAASO J1219+2915 in the first Large High Altitude Air Shower Observatory (LHAASO) source catalog. However, no associated counterpart has been detected by Fermi-LAT. By analyzing its X-ray observation data from Swift-XRT, we find it is in a high-flux state on MJD 59546, with the X-ray flux more than one order of magnitude higher than that observed ~ 11.7 year earlier by Chandra. We propose that the detection of VHE γ -rays from NGC 4278 may be attributed to the presence of an active nucleus displaying behavior similar to that of a BL Lac. To reproduce its spectral energy distribution (SED), we employ a one-zone leptonic model, typically used for fitting broadband SEDs of BL Lacs, and find that smaller values for both Doppler factor (δ) and magnetic field strength (B) are required than that of typical TeV BL Lacs. Furthermore, NGC 4278 exhibits significantly lower luminosity in both radio and TeV bands when compared with typical TeV BL Lacs. In the radio-luminosity vs. Eddington-ratio plane, NGC 4278 shows greater similarity to Seyfert galaxies and LINERs rather than BL Lacs; however, it still roughly follows the extension towards lower luminosity seen in BL Lacs.

Keywords: astroparticle physics – gamma rays: galaxies – galaxies: active – galaxies: individual (NGC 4278)

1. INTRODUCTION

Radio-loud active galactic nuclei (RL-AGNs) account for about 15% – 20% of the AGN population (Urry & Padovani 1995), characterized as the powerful relativistic jet radiations. Blazars, a special type of RL-AGNs, have their jets pointing nearly along the line of sight and are divided into BL Lacertae objects (BL Lacs) and flat spectrum radio quasars (FSRQs) based on their emission line features in the optical band (Scarpa & Falomo 1997). Blazars are the main extragalactic gigaelectronvolt-teraelectronvolt (GeV–TeV) γ -ray emitting objects, especially in the TeV band. In recent years, many other types of RL-AGNs have been confirmed as γ -ray emitters. For example, radio galaxies (Abdollahi et al. 2020), Narrow-line Seyfert 1 galaxies (NLS1s, Abdo et al. 2009; Sun et al. 2015), compact steep-spectrum sources (CSSs, Abdollahi et al. 2020; Zhang et al. 2020), compact symmetric objects (CSOs, Migliori et al. 2016; Principe et al. 2020; Lister et al. 2020; Gan et al. 2021, 2022, 2024), and

low-luminosity FR0 type radio galaxies (Grandi et al. 2016; Fu et al. 2022). The large-scale extended regions of jets in AGNs also have been confirmed to emit detectable γ -rays (Abdo et al. 2010; Ackermann et al. 2016; Yu et al. 2024). It is worth noting that in the TeV band, apart from several FSRQs and radio galaxies, BL Lacs are the main type of detected extragalactic γ -ray emitting AGNs¹.

Recently, the Large High Altitude Air Shower Observatory (LHAASO) collaboration reported their first catalog (Cao et al. 2024). One new extragalactic TeV γ -ray emitting source was presented. The point-like source 1LHAASO J1219+2915 located at high Galactic Latitude was detected with a test statistic of $TS=49.2$ and suggested to be associated with the AGN NGC 4278. The distance between NGC 4278 and 1LHAASO J1219+2915 is 0.05° . NGC 4278 is previously classified as a low-ionization nuclear emission line region (LINER, Heckman 1980). No AGNs of this type have been detected in the γ -ray band.

NGC 4278, located at $z = 0.00216$ (González-Martín et al. 2009), belongs to an RL-AGN. However, the total radio lumi-

Corresponding author: Jin Zhang
j.zhang@bit.edu.cn

¹ <http://tevcat2.uchicago.edu/>

osity of NGC 4278 is at least 2 orders of magnitude less than the typical RL-AGNs (Condon et al. 1998). The Very Long Baseline Array (VLBA) has resolved its two-sided symmetric steep-spectrum jets on a sub-parsec scale emerging from a flat-spectrum core region (Giroletti et al. 2005). Its radio flux density at 6 cm between 1972 and 2003 exhibits significant variability ($\geq 100\%$) on timescale of years, and the outburst around 1985 may be related to the presence of an active nucleus (Giroletti et al. 2005). In the UV band, its nucleus is barely resolved and exhibits evident variability. Its UV flux increases by a factor of 1.6 during a period of 6 months, and the observed UV flare features, amplitude and scale time, are prominently similar to that observed in other low-luminosity AGNs (LLAGNs, Cardullo et al. 2009). Using the Space Telescope Imaging Spectrograph, Cardullo et al. (2009) obtained spectra of the nucleus, measured the broad components of the emission lines, and estimated the mass of the central supermassive black hole (SMBH) to be in the range of $7 \times 10^7 - 2 \times 10^9 M_{\odot}$. In X-rays, no evident short time-scale (hours and days) variability is observed in the nucleus of NGC 4278 during the Chandra observations. However, an increase in flux by a factor of 10% is observed over a period of 1 hour during the XMM-Newton observation. Younes et al. (2010) also reported that the nucleus flux in NGC 4278 increases by a factor of 3 over a few months and by a factor of 5 between the faintest and brightest observations separated by ~ 3 years. Additionally, NGC 4278 hosts numerous resolved low-mass X-ray binaries (LMXBs), more than one hundred of which exhibit long-term variability (Brassington et al. 2009). In γ -rays, apart from a transient source, namely 1FLT J1219+2907, reported by the Fermi-LAT transient sources catalog with its position consistent with NGC 4278 from 2009 March 5 to 2009 April 5 (Baldini et al. 2021), no other high-energy γ -rays have been detected. Therefore, the origin of the detected γ -ray emission from 1LHAASO J1219+2915 associated with NGC 4278 is confusing.

In this paper, we aim to study the radiation physics and the origin of VHE γ -rays from NGC 4278 by analysing its observational data in multiwavelength. Data analysis of Fermi-LAT, Chandra, and Swift-XRT is presented in Section 2. In Section 3, we describe the X-ray emission property of the nucleus in NGC 4278. The construction and modeling of the broadband spectral energy distribution (SED) for the nucleus of NGC 4278 are presented in Section 4. Discussion on the origin of VHE γ -rays and the AGN type of NGC 4278 is given in Section 5, while a summary is provided in Section 6. Throughout, the cosmological parameters $H_0 = 70 \text{ km s}^{-1} \text{ Mpc}^{-1}$, $\Omega_m = 0.3$, and $\Omega_{\Lambda} = 0.7$ are adopted.

2. OBSERVATIONS AND DATA REDUCTION

2.1. Fermi-LAT

We investigate the latest Fermi-LAT 14 yr Source Catalog (4FGL-DR4, Abdollahi et al. 2022; Ballet et al. 2023) and find only two γ -ray sources located within a 1° radius circle centered on the radio position of NGC 4278, namely 4FGL J1221.3+3010 and 4FGL J1217.9+3007. They are 0.929° and 0.964° distance from NGC 4278, and are associated with BL Lacs IES 1218+304 and B2 1215+30, respectively. Both of these two BL Lacs have been detected in the TeV band and have been confirmed as TeV γ -ray emitters (Albert et al. 2006; Acciari et al. 2009; Aleksić et al. 2012; Aliu et al. 2013).

To further investigate if there are γ -ray emission from Fermi-LAT associated with NGC 4278, the Pass 8 data, covering ~ 16 yr from 2008 August 4 to 2024 April 24 (MJD 54682–60424), are extracted from Fermi Science Support Center² for our analysis. We select the region of interest (ROI) centered at the radio position of NGC 4278 (R.A.=185.028°, Decl.=29.281°) with a radius of 15° . The publicly available software `Fermitools` (version 2.2.0) are used for our analysis. We use event class “SOURCE” (evclass=128) and event type “FRONT+BACK” (evtype=3) for data analysis based on LAT data selection recommendations. The γ -ray events in the energy range of 0.1–300 GeV are selected with a standard data quality selection criteria of “(DATA_QUAL>0)&&(LAT_CONFIG==1)”. The instrument response function of “P8R3_SOURCE_V3” (Bruel et al. 2018) is used. A maximum zenith angle of 90° is set to reduce the γ -ray contamination from the Earth limb. The background model in the ROI includes the isotropic background model `iso_P8R3_V3_v1.txt` and the diffuse Galactic interstellar emission with the parameterized model `gll_iem_v07.fits`, as well as all the γ -ray sources listed in the 4FGL-DR4. The normalization of the isotropic background emission and the diffuse Galactic interstellar emission, together with the normalization and spectral parameters of the γ -ray point sources within a 6.5° radius centered on NGC 4278, are left free, whereas the parameters of those point sources lying beyond 6.5° are fixed to their 4FGL-DR4 values.

The maximum likelihood test statistic (TS) is used to quantify the significance of the detection of γ -ray sources, which is defined as $TS = 2 \log(\frac{\mathcal{L}_{\text{src}}}{\mathcal{L}_{\text{null}}})$ (Mattox et al. 1996), where \mathcal{L}_{src} and $\mathcal{L}_{\text{null}}$ are the maximum likelihood values for the background with and without a source, respectively. If $TS \geq 25$, it indicates that there is a new source. We generate a $5^\circ \times 5^\circ$ residual TS map centered on the radio position of NGC 4278, and find that the maximum TS value in the residual TS map is ~ 13 . Therefore, no new γ -ray source is

² <https://fermi.gsfc.nasa.gov/ssc/data/access/>

observed, indicating that no GeV γ -ray emission from NGC 4278 is detected.

2.2. Chandra

NGC 4278 has been observed by the Chandra observatory using the Advanced CCD Imaging Spectrometer S-array (ACIS-S) in nine epochs. The shortest and longest exposure times are 1.4 ks and 110.7 ks, as listed in Table 1. The first seven observations (Obs-ID: 398, 4741, 7077, 7078, 7079, 7080, 7081) have been analyzed by [Younes et al. \(2010\)](#), and they found that all of these observations suffered the pile-up effect, with a pile-up fraction of $> 5\%$. The first Chandra snapshot observation (Obs-ID: 398) with the short exposure time cannot produce a useful spectrum after considering the pile-up effect ([Younes et al. 2010](#)), and thus it is excluded.

In this paper, we only analyze the last two observation data from Chandra. The data are reduced with CIAO (v.4.15) and CALDB (v.4.10.4), and then we generate the level-2 event file in a standard procedure. We firstly check the pile-up effect of the two observations by creating pile-up maps with a CIAO tool of `pileup_map`³. No pixel has the count rate per frame greater than 0.1 (corresponding to a pile-up fraction of $> 5\%$), indicating no pile-up effect in the last two observations. We then extract the source photons from a circle centered on the radio position of NGC 4278 with a radius of $7''$. The background is taken from an annulus region with inner and outer radii of $10''$ and $20''$, respectively. The spectrum is grouped to have at least 15 counts per bin and the χ^2 minimization technique is used for the spectral analysis. The spectral fitting is performed using XSPEC (v.12.13.0c). We use the same model adopted in [Younes et al. \(2010\)](#) to fit the spectra in the energy range of 0.5–8.0 keV, i.e., a single power-law absorbed by Galactic and host galaxy plus a thermal component (`mekal` in XSPEC). The neutral hydrogen column density of Galactic ($N_{\text{gal}}^{\text{H}}$) is fixed as $2.07 \times 10^{20} \text{ cm}^{-2}$ ([Kalberla et al. 2005](#)) while the value of host galaxy ($N_{\text{int}}^{\text{H}}$) is set to be free. The fitting parameters of the two spectra are given in Table 1 and the results of the first seven observations reported in [Younes et al. \(2010\)](#) are also presented in the table for comparison. The derived temperatures of the thermal component in the two spectra are almost identical to that reported in [Younes et al. \(2010\)](#). However, we can only obtain an upper limit of $N_{\text{int}}^{\text{H}}$ for the two observations.

2.3. Swift-XRT

Swift X-Ray Telescope (Swift-XRT) has performed 4 observations to NGC 4278 in the Photon Counting readout mode between 2017 December and 2021 November. However, the radio position of NGC 4278 is outside of the XRT's

view field during two observations. Therefore, only the other two sets of observational data are used in our analysis; one observation was on 2021 Feb 26 (MJD 59271) with an exposure time of 173 s and another observation was on 2021 Nov 28 (MJD 59546) with an exposure time of 923 s. It is worth noting that the observational data from MJD 59271 have a minimal impact on the spectral fit due to their short exposure time. The result of spectral fit is primarily influenced by the observational data from MJD 59546. The data are processed using the XRTDAS software package (v.3.7.0). The software package was developed by the ASI Space Science Data Center and released by the NASA High Energy Astrophysics Science Archive Research Center (HEASARC) in the HEASoft package (v.6.30.1). The calibration files from XRT CALDB (version 20220803) are used within `xrtpipeline` to calibrate and clean the events. Considering the short exposure time of the two observations, we merge the two XRT event files together using the `xselect` package and produce a combined average spectrum. The source photons are extracted from a circle centered on the radio position of NGC 4278 with a radius of 20 pixels ($\sim 47''$). The background is taken from an annulus with an inner and outer radii of 30 pixels ($\sim 71''$) and 45 pixels ($\sim 106''$), respectively. The combined average spectrum is grouped to have at least 4 counts per bin. We use the public software XSPEC (v.12.13.0c) to fit the spectrum and the C-statistic minimization is adopted for evaluating the goodness of the fits. The energy channels below 0.5 keV and above 8 keV are excluded during fitting. Same as the data analysis of Chandra, the spectrum is fitted by a single power-law absorbed by two absorption components; the neutral hydrogen column density of Galactic is fixed at $N_{\text{gal}}^{\text{H}} = 2.07 \times 10^{20} \text{ cm}^{-2}$ ([Kalberla et al. 2005](#)) while the neutral hydrogen column density of host galaxy ($N_{\text{int}}^{\text{H}}$) is set to be free. We obtain a C-statistic value/d.o.f of 3.51/6 and calculate the corrected flux in the energy range of 0.5 – 8.0 keV, as listed in Table 1.

3. X-RAY EMISSION OF THE NUCLEUS IN NGC 4278

The X-ray light curve of NGC 4278 is compiled in Figure 1, incorporating the archived X-ray data from [Younes et al. \(2010\)](#) and the analysis results from the Chandra and Swift-XRT observations conducted in this study. Notably, NGC 4278 exhibits significant flux variations in the X-ray band. During the observation on MJD 59546, Swift-XRT detected a remarkably high-flux state for NGC 4278 in the X-ray band, surpassing even the historically highest flux obtained from XMM-Newton observation on 2004 May 23. The ratio between the highest flux observed by Swift-XRT in 2021 and the lowest flux observed by Chandra in 2010 exceeds one order of magnitude. Unfortunately, no additional data between 2010 to 2021 could be acquired to estimate variability timescales accurately. While previous studies have reported

³ https://cxc.harvard.edu/ciao/ahelp/pileup_map.html

a $\sim 10\%$ increase in flux over a period of ~ 1 hr during XMM-Newton observations (Younes et al. 2010), due to limited exposure time during the Swift-XRT observations, further investigation into short timescale variability is not feasible in this study.

The compact and symmetric two-sided radio morphology of NGC 4278 fulfills the criteria for classification as a CSO, and it is even included in a ‘bona fide’ CSO sample (Kiehlmann et al. 2024). CSOs may be transient or episodic sources (O’Dea & Saikia 2021 for a review), with some γ -ray emitting CSOs reported to display episodic nuclear activity (Lister et al. 2020; Gan et al. 2021, 2022). It should be noted that radio observations at 6 cm from 1972 to 2003 indicate variability in the flux density of NGC 4278, including an observed outburst around 1985, which may be associated with the presence of an active nucleus (Giroletti et al. 2005). Therefore, the high-flux state observed in X-rays for NGC 4278 could potentially be attributed to the reactivation of its nucleus once again around 2021. This may be the reason that NGC 4278 has recently been detected at the VHE γ -ray band by LHAASO.

The photon spectral index (Γ_X) against the X-ray flux is depicted in Figure 2. Despite the presence of large errors in the data points, significant spectral variations can still be observed. NGC 4278 shows the *harder when brighter* behavior, which is commonly observed among BL Lacs in the X-ray band (e.g., Tramacere et al. 2009; Tramacere et al. 2011; Zhang et al. 2013; Di Gesu et al. 2022; Hu et al. 2024).

4. CONSTRUCTING AND MODELING THE SED OF NUCLEUS

The reactivation of the nucleus, as mentioned above, likely result in the detection of VHE γ -rays and a high-flux state in X-rays from NGC 4278. Consequently, it is plausible that both the emission in X-rays and γ -rays originate from the same region. In order to further investigate the γ -ray emission properties of NGC 4278, we collect its multiwavelength observation data from literature and construct a broadband SED. However, only a few non-simultaneous observations from Younes et al. (2010) are available in the radio-optical-UV bands, as shown in Figure 3. The sensitivity curves of LHAASO (Wang et al. 2022), VERITAS (Bigongiari & CTA Consortium 2016), and Fermi-LAT (Funk et al. 2013) are also presented in Figure 3. The hard X-ray spectrum and soft TeV γ -ray spectrum should correspond to two distinct radiation components, resembling those typical TeV-emitting BL Lacs that have a high synchrotron radiation peak (e.g., Zhang et al. 2012). We employ a simple one-zone leptonic model, widely used in modeling the broadband SEDs of TeV BL Lacs (e.g., Zhang et al. 2012; Yan et al. 2014), to reproduce the SED of NGC 4278, only considering

synchrotron and synchrotron-self-Compton (SSC) processes of the relativistic electrons.

The electron distribution is taken as a broken power law,

$$N(\gamma) = N_0 \begin{cases} \gamma^{-p_1} & \gamma_{\min} \leq \gamma \leq \gamma_b, \\ \gamma_b^{p_2-p_1} \gamma^{-p_2} & \gamma_b < \gamma < \gamma_{\max}. \end{cases} \quad (1)$$

The emission region is assumed as a sphere with radius R , magnetic field B , and a Doppler boosting factor δ , where R is taken as $R = c\Delta t\delta/(1+z)$. BL Lacs generally show variability on daily or hour timescales (e.g., Xie et al. 2001; Ravasio et al. 2002; Błażejowski et al. 2005; Fossati et al. 2008; Acciari et al. 2011; Nalewajko 2013), we thus take $\Delta t = 1$ day for NGC 4278. The VLBA observations indicate that NGC 4278 has mildly relativistic jets ($\beta \sim 0.75$) with a viewing angle of $2^\circ \sim 4^\circ$, which result in a Doppler boosting factor of 2.7 (Giroletti et al. 2005). We thus fix δ to be 2.7. The values of p_1 and p_2 are constrained by the spectral indices at X-ray and TeV bands. Since γ_{\min} cannot be constrained and is fixed as $\gamma_{\min} = 1$, while γ_{\max} is poorly constrained by the last observation point at TeV band. We adjust the parameters B , N_0 , and γ_b to represent the observed SED of NGC 4278. No detection of VHE γ -rays from NGC 4278 has been reported by other TeV detectors; therefore, we consider the sensitivity curve of VERITAS as an upper limit during SED modeling. The Klein–Nishina effect (Ghisellini et al. 1998) and the absorption of extragalactic background light (EBL; Finke et al. 2022) are also taken into account in the SED modeling. The SED fitting parameters are given in table 2.

Reproducing the SED of NGC 4278, we obtain $B = 0.015$ G, $\gamma_b = 4 \times 10^6$, and $N_0 = 3.5 \times 10^4 \text{ cm}^{-3}$. It should be noted that the fitting parameters B and δ are degenerate (Zhang et al. 2012). If a high magnetic field strength is required to represent the broadband SED of NGC 4278, then a smaller δ . For example, $\delta = 1$ would be necessary with $B = 0.2$ G. Based on these SED fitting parameters, we also calculate the jet power ($P_{\text{jet}}^{e^\pm}$) in case of the e^\pm pair jet for NGC 4278 by assuming that the jet consist of electrons (P_e), magnetic fields (P_B), and radiation (P_r). The corresponding values are $6.97 \times 10^{42} \text{ erg s}^{-1}$, $5.99 \times 10^{38} \text{ erg s}^{-1}$, and $5.56 \times 10^{41} \text{ erg s}^{-1}$, respectively (see Table 2).

5. DISCUSSION

The angular resolution of LHAASO can achieve $< 1^\circ$ around 10 TeV (Ma et al. 2022). As stated in Section 2.1, there are two other GeV-TeV BL Lacs located within a distance of less than 1° from NGC 4278. Moreover, NGC 4278 harbors a substantial number of LMXBs (Brassington et al. 2009; D’Abrusco et al. 2014), and γ -rays have been observed from several LMXBs in the Galaxy. We are wondering whether the VHE γ -rays detected by LHAASO from 1LHAASO J1219+2915 could potentially originate from ei-

ther the two γ -ray emitting BL Lacs or these LMXBs in NGC 4278.

5.1. Two TeV BL Lacs Located near NGC 4278

The GeV-TeV emitting BL Lacs 1ES 1218+304 and B2 1215+30 are situated at a distance of 0.929° and 0.964° , respectively, from the radio position of NGC 4278. Firstly, we conduct a literature search to identify the highest observed flux at the TeV band for the two BL Lacs. We then extrapolate their intrinsic γ -ray spectrum up to 100 TeV assuming a power-law spectral form. Subsequently, we calculate the observable spectral shape by taking into account the absorption of EBL and compare it with that of 1LHAASO J1219+2915. Two EBL models are considered in this analysis, corresponding to the strongest absorption (Franceschini & Rodighiero 2017) and weakest absorption (Kneiske & Raue 2010), respectively.

For 1ES 1218+304, located at a redshift of $z = 0.182$ (Véron-Cetty & Véron 2003), the intrinsic γ -ray spectrum in the TeV band is taken from Acciari et al. (2009). We extrapolate this intrinsic γ -ray spectrum to higher energy bands by assuming a power-law spectral shape, and subsequently derive the observable spectrum in the TeV band by taking into account the absorption of EBL, as illustrated in Figure 4(a). For B2 1215+30, we obtain the observed spectrum in the TeV band from Abeysekara et al. (2017). Considering that there is uncertainty regarding its redshift, i.e., either $z = 0.130$ (Akiyama et al. 2003) or $z = 0.237$ (Lanzetta et al. 1993), we consider both cases. Firstly, we correct for EBL absorption on the observation data using both strongest and weakest EBL models to obtain an intrinsic γ -ray spectrum and extrapolate this obtained intrinsic γ -ray spectrum up to 100 TeV (the blue and magenta solid lines in Figure 4) by assuming a power-law spectral form. Subsequently, considering again the effect of EBL absorption, we calculate the observable flux in the TeV band, represented by the blue and magenta dashed lines shown in Figures 4(b) and 4(c).

The LHAASO is capable of detecting both 1ES 1218+304 and B2 1215+30 when they are in a high-flux state, as depicted in Figures 4. However, the estimated observable spectra of the two BL Lacs fail to represent the observed highest energy photon of 1LHAASO J1219+2915 when considering the strongest EBL absorption model. In other words, due to their high redshift, it appears impossible for the LHAASO to detect γ -ray photons with energies exceeding 10 TeV from the two BL Lacs, even when considering the weakest EBL absorption model. Therefore, the VHE γ -ray emission from 1LHAASO J1219+2915 should not be contributed by the two BL Lacs.

5.2. LMXBs in NGC 4278

Several Galactic LMXBs have been detected at the γ -ray band (e.g., Xing & Wang 2015; Harvey et al. 2022a;

Harvey et al. 2022b; Kantzas et al. 2022). In NGC 4278, there exist multiple LMXBs with an X-ray luminosity exceeding 10^{38} erg s $^{-1}$ (Brassington et al. 2009; Fabbiano et al. 2010), which are likely to be sources of γ -ray emission as well. Therefore, we estimate the potential γ -ray flux from these LMXBs in NGC 4278 by assuming that they exhibit a similar X-ray to γ -ray flux ratio as the Galactic γ -ray emitting LMXBs, i.e.,

$$\frac{F_{\gamma,\text{LMXB}}}{F_{\text{X,LMXB}}} = \frac{F_{\gamma,\text{J1023}}}{F_{\text{X,J1023}}}, \quad (2)$$

where $F_{\gamma,\text{LMXB}}$ and $F_{\text{X,LMXB}}$ are the fluxes at γ -ray and X-ray bands of the LMXBs in NGC 4278, $F_{\gamma,\text{J1023}}$ and $F_{\text{X,J1023}}$ are the γ -ray and X-ray fluxes of the LMXB PSR J1023+0038. PSR J1023+0038 is a well observed Galactic γ -ray emitting LMXB. The observational data for PSR J1023+0038 are obtained from Li et al. (2014) and Xing et al. (2018), as shown in Figure 5 (black symbols). Taking $F_{\text{X,J1023}} = 4.01 \times 10^{-13}$ erg cm $^{-2}$ s $^{-1}$ in the 0.5–10 keV band (Campana et al. 2016) and $F_{\text{X,LMXB}} = 7.79 \times 10^{-14}$ erg cm $^{-2}$ s $^{-1}$ in the 0.3–8 keV band (Fabbiano et al. 2010), where the maximum value of $F_{\text{X,LMXB}}$ among these LMXBs in NGC 4278 is considered, the γ -ray fluxes of the brightest LMXB in NGC 4278 can be estimated as $F_{\gamma,\text{LMXB}} = 0.19F_{\gamma,\text{J1023}}$.

We extrapolate the GeV spectrum of PSR J1023+0038 up to the TeV band by assuming they follow the same power-law distribution (the black solid line in Figure 5). Multiplying the black solid line by 0.19, we obtain the possible γ -ray flux (the blue solid line) of the brightest LMXB in NGC 4278. The blue dashed line in Figure 5 presents the result after considering EBL absorption. It is evident that if there is only one γ -ray emitting LMXB in NGC 4278, its emission would not be detectable by Fermi-LAT and VERITAS but could potentially be detected by LHAASO. NGC 4278 hosts several LMXBs with X-ray luminosities exceeding 10^{38} erg s $^{-1}$, some of which exhibit significant variability (Fabbiano et al. 2010). Therefore, it is plausible that the observed γ -rays from 1LHAASO J1219+2915 can be attributed to some LMXBs in NGC 4278. However, no detection has been made for any LMXB at TeV energy band.

In addition, the spectrum at the TeV band of LMXB may not follow the same power-law spectral shape as that at the GeV band; a flatter spectrum is observed in high-mass X-ray binaries (HMXBs) at the TeV band, for example, HESS J1018–589 A/1FGL J1018.6–5856 (H. E. S. S. Collaboration et al. 2015). Considering the presence of multiple bright LMXBs in NGC 4278, we cannot dismiss the possibility that the detection of 1LHAASO J1219+2915 could be attributed to these LMXBs within NGC 4278.

5.3. NGC 4278: a BL Lac or a LINER

The compact radio morphology and flat radio spectrum of NGC 4278 suggest its similarity to BL Lacs (Giroletti et al. 2005). The SED of NGC 4278 can be represented by a one-zone synchrotron+SSC model, similar to the typical TeV BL Lacs. We compare the derived jet physical parameters of NGC 4278 with that of a TeV-BL Lac sample from Zhang et al. (2012). It seems that NGC 4278 does not fit in with the characteristics of those typical TeV BL Lacs. As shown in Figure 6, both the B and δ values for NGC 4278 are considerably smaller, while γ_b is slightly larger compared to typical TeV BL Lacs. In the $P_{\text{jet}}^{\pm} - P_r$ plane (Figure 7), NGC 4278 well follows the sequence of typical TeV BL Lacs but resides at the low-power end. Nevertheless, when examining the $P_{\text{jet}}^{\pm} - P_B$ plane, it becomes evident that NGC 4278 stands apart from these TeV BL Lacs due to an unusually smaller ratio of P_B to P_{jet}^{\pm} .

To further investigate this issue, we compile the radio luminosity at 8 GHz ($L_{8 \text{ GHz}}$) of NGC 4278 and these typical TeV BL Lacs from the Radio Fundamental Catalog (RFC)⁴, and plot the γ -ray luminosity at 1 TeV ($L_{1 \text{ TeV}}$) against $L_{8 \text{ GHz}}$ in Figure 8(a). No significant correlation between $L_{8 \text{ GHz}}$ and $L_{1 \text{ TeV}}$ for these typical TeV BL Lacs is observed. Moreover, NGC 4278 stands out as it is clearly separated from these typical BL Lacs and positioned at the lower end of the luminosity scale. The luminosity of NGC 4278 is more than two orders of magnitude lower than that of typical TeV BL Lacs in both radio and γ -ray bands.

As described above, NGC 4278 does exhibit distinctive characteristics that differentiate it from typical TeV BL Lacs, and it is generally classified as a LINER (Heckman 1980) or a ‘bona fide’ CSO (Kiehlmann et al. 2024). In Figure 8(b), we plot the radio luminosity (L_R) against the Eddington ratio (R_{Edd}) for a sample of Seyfert galaxies and LINERs from Sikora et al. (2007), as well as for a sample of BL Lacs from Zhang et al. (2020). Note that the BL Lac sample in Figure 8(b) differs partially from that in Figure 8(a). Not all BL Lacs shown in Figure 8(b) are TeV sources, and not all BL Lacs depicted in Figure 8(a) have available R_{Edd} data. However, there is an overlap between the two samples. For Seyfert galaxies and LINERs, L_R represents the luminosity at 5 GHz, while for NGC 4278 and these BL Lacs it corresponds to $L_{8 \text{ GHz}}$, where the $L_{8 \text{ GHz}}$ values are also derived from the observation data obtained in RFC. Both samples (neither considering NGC 4278) show a clear correlation between L_R and R_{Edd} . The Pearson correlation analysis yields a coefficient $r = 0.629$ and a chance probability $p = 2.34 \times 10^{-5}$ for all Seyfert galaxies and LINERs, while $r = 0.769$ and $p = 1.17 \times 10^{-4}$ are obtained for these BL Lacs. In the $R_{\text{Edd}} - L_R$ plane, NGC 4278 is situated within

the region occupied by Seyfert galaxies and LINERs, slightly deviating from the low-luminosity extension of the 95% confidence band of the best linear fit for BL Lacs. The Eddington ratio of NGC 4278 is more than one order of magnitude lower than that of BL Lacs, which may be the reason for its low luminosity. Considering all these aspects, NGC 4278 does not resemble a BL Lac; instead, it exhibits more similarities to Seyfert galaxies and LINERs.

6. SUMMARY

NGC 4278 was classified as a LINER-type AGN and no associated γ -ray source counterpart reported in the 4FGL-DR4 (Abdollahi et al. 2022; Ballet et al. 2023). By reanalyzing all the Fermi-LAT observation data from 2008 Aug 4 to 2024 Apr 24 around the radio position of NGC 4278, no significant γ -ray emission associated with NGC 4278 is found. Interestingly, NGC 4278 has been detected by LHAASO and is reported to be associated with 1LHAASO J1219+2915 (Cao et al. 2024). To investigate the origin of VHE emission from this source, we examine its X-ray observations obtained by Swift-XRT, Chandra, and XMM-Newton, and find only one valid pointing (on MJD 59546) from Swift-XRT during the LHAASO observations. Surprisingly, the derived X-ray flux from Swift-XRT is more than one order of magnitude higher than the archive X-ray flux obtained by Chandra observation ~ 11.7 years ago, indicating that the X-ray emission of NGC 4278 is currently in a historically high-flux state. Together with the mildly relativistic jets detected in the radio band using the VLBA observations, we propose that the TeV γ -rays of 1LHAASO J1219+2915 originate from an atypical BL Lac-type AGN in the center of NGC 4278 that has recently become more active; however, other possibilities cannot be completely ruled out yet. The derived parameters for its jet using a one-zone synchrotron+SSC model are also significantly different from that of these typical TeV BL Lacs, with smaller δ and B , but higher energies of electrons. In both radio and TeV bands, NGC 4278 shows luminosity lower by over two orders of magnitude when compared to these typical TeV BL Lacs. In the $R_{\text{Edd}} - L_R$ plane, NGC 4278 slightly deviates from the low-luminosity and low-Eddington-ratio extension of the 95% confidence band representing best linear fit for BL Lacs; instead it exhibits similarities with Seyfert galaxies and LINERs.

ACKNOWLEDGMENTS

We acknowledge the use in our research the Radio Fundamental Catalogue available at <https://astrogeo.smce.nasa.gov/rfc/>. This work is supported by the National Key R&D Program of China (grant 2023YFE0117200) and the National Natural Science Foundation of China (grants 12022305 and 11973050).

⁴ <https://astrogeo.smce.nasa.gov/rfc/>

REFERENCES

- Abdo, A. A., Ackermann, M., Ajello, M., et al. 2009, *ApJL*, 707, L142, doi: [10.1088/0004-637X/707/2/L142](https://doi.org/10.1088/0004-637X/707/2/L142)
- . 2010, *Science*, 328, 725, doi: [10.1126/science.1184656](https://doi.org/10.1126/science.1184656)
- Abdollahi, S., Acero, F., Ackermann, M., et al. 2020, *ApJS*, 247, 33, doi: [10.3847/1538-4365/ab6bcb](https://doi.org/10.3847/1538-4365/ab6bcb)
- Abdollahi, S., Acero, F., Baldini, L., et al. 2022, *ApJS*, 260, 53, doi: [10.3847/1538-4365/ac6751](https://doi.org/10.3847/1538-4365/ac6751)
- Abeyssekara, A. U., Archambault, S., Archer, A., et al. 2017, *ApJ*, 836, 205, doi: [10.3847/1538-4357/836/2/205](https://doi.org/10.3847/1538-4357/836/2/205)
- Acciari, V. A., Aliu, E., Arlen, T., et al. 2009, *ApJ*, 695, 1370, doi: [10.1088/0004-637X/695/2/1370](https://doi.org/10.1088/0004-637X/695/2/1370)
- . 2011, *ApJ*, 738, 169, doi: [10.1088/0004-637X/738/2/169](https://doi.org/10.1088/0004-637X/738/2/169)
- Ackermann, M., Ajello, M., Baldini, L., et al. 2016, *ApJ*, 826, 1, doi: [10.3847/0004-637X/826/1/1](https://doi.org/10.3847/0004-637X/826/1/1)
- Akiyama, M., Ueda, Y., Ohta, K., Takahashi, T., & Yamada, T. 2003, *ApJS*, 148, 275, doi: [10.1086/376441](https://doi.org/10.1086/376441)
- Albert, J., Aliu, E., Anderhub, H., et al. 2006, *ApJL*, 642, L119, doi: [10.1086/504845](https://doi.org/10.1086/504845)
- Aleksić, J., Alvarez, E. A., Antonelli, L. A., et al. 2012, *A&A*, 544, A142, doi: [10.1051/0004-6361/201219133](https://doi.org/10.1051/0004-6361/201219133)
- Aliu, E., Archambault, S., Arlen, T., et al. 2013, *ApJ*, 779, 92, doi: [10.1088/0004-637X/779/2/92](https://doi.org/10.1088/0004-637X/779/2/92)
- Baldini, L., Ballet, J., Bastieri, D., et al. 2021, *ApJS*, 256, 13, doi: [10.3847/1538-4365/ac072a](https://doi.org/10.3847/1538-4365/ac072a)
- Ballet, J., Bruel, P., Burnett, T. H., Lott, B., & The Fermi-LAT collaboration. 2023, arXiv e-prints, arXiv:2307.12546, doi: [10.48550/arXiv.2307.12546](https://doi.org/10.48550/arXiv.2307.12546)
- Bigongiari, C., & CTA Consortium. 2016, *Nuclear and Particle Physics Proceedings*, 279-281, 174, doi: [10.1016/j.nuclphysbps.2016.10.025](https://doi.org/10.1016/j.nuclphysbps.2016.10.025)
- Błaziejowski, M., Blaylock, G., Bond, I. H., et al. 2005, *ApJ*, 630, 130, doi: [10.1086/431925](https://doi.org/10.1086/431925)
- Brassington, N. J., Fabbiano, G., Kim, D. W., et al. 2009, *ApJS*, 181, 605, doi: [10.1088/0067-0049/181/2/605](https://doi.org/10.1088/0067-0049/181/2/605)
- Bruel, P., Burnett, T. H., Digel, S. W., et al. 2018, arXiv e-prints, arXiv:1810.11394, doi: [10.48550/arXiv.1810.11394](https://doi.org/10.48550/arXiv.1810.11394)
- Campana, S., Coti Zelati, F., Pappitto, A., et al. 2016, *A&A*, 594, A31, doi: [10.1051/0004-6361/201629035](https://doi.org/10.1051/0004-6361/201629035)
- Cao, Z., Aharonian, F., An, Q., et al. 2024, *ApJS*, 271, 25, doi: [10.3847/1538-4365/acfd29](https://doi.org/10.3847/1538-4365/acfd29)
- Cardullo, A., Corsini, E. M., Beifiori, A., et al. 2009, *A&A*, 508, 641, doi: [10.1051/0004-6361/200913046](https://doi.org/10.1051/0004-6361/200913046)
- Condon, J. J., Yin, Q. F., Thuan, T. X., & Boller, T. 1998, *AJ*, 116, 2682, doi: [10.1086/300624](https://doi.org/10.1086/300624)
- D'Abrusco, R., Fabbiano, G., & Brassington, N. J. 2014, *ApJ*, 783, 19, doi: [10.1088/0004-637X/783/1/19](https://doi.org/10.1088/0004-637X/783/1/19)
- Di Gesu, L., Donnarumma, I., Tavecchio, F., et al. 2022, *ApJL*, 938, L7, doi: [10.3847/2041-8213/ac913a](https://doi.org/10.3847/2041-8213/ac913a)
- Fabbiano, G., Brassington, N. J., Lentati, L., et al. 2010, *ApJ*, 725, 1824, doi: [10.1088/0004-637X/725/2/1824](https://doi.org/10.1088/0004-637X/725/2/1824)
- Finke, J. D., Ajello, M., Domínguez, A., et al. 2022, *ApJ*, 941, 33, doi: [10.3847/1538-4357/ac9843](https://doi.org/10.3847/1538-4357/ac9843)
- Fossati, G., Buckley, J. H., Bond, I. H., et al. 2008, *ApJ*, 677, 906, doi: [10.1086/527311](https://doi.org/10.1086/527311)
- Franceschini, A., & Rodighiero, G. 2017, *A&A*, 603, A34, doi: [10.1051/0004-6361/201629684](https://doi.org/10.1051/0004-6361/201629684)
- Fu, W.-J., Zhang, H.-M., Zhang, J., et al. 2022, *Research in Astronomy and Astrophysics*, 22, 035005, doi: [10.1088/1674-4527/ac4410](https://doi.org/10.1088/1674-4527/ac4410)
- Funk, S., Hinton, J. A., & CTA Consortium. 2013, *Astroparticle Physics*, 43, 348, doi: [10.1016/j.astropartphys.2012.05.018](https://doi.org/10.1016/j.astropartphys.2012.05.018)
- Gan, Y.-Y., Zhang, H.-M., Yang, X., Gu, Y., & Zhang, J. 2024, *Research in Astronomy and Astrophysics*, 24, 025018, doi: [10.1088/1674-4527/ad1c78](https://doi.org/10.1088/1674-4527/ad1c78)
- Gan, Y.-Y., Zhang, H.-M., Zhang, J., et al. 2021, *Research in Astronomy and Astrophysics*, 21, 201, doi: [10.1088/1674-4527/21/8/201](https://doi.org/10.1088/1674-4527/21/8/201)
- Gan, Y.-Y., Zhang, J., Yao, S., et al. 2022, *ApJ*, 939, 78, doi: [10.3847/1538-4357/ac9589](https://doi.org/10.3847/1538-4357/ac9589)
- Ghisellini, G., Celotti, A., Fossati, G., Maraschi, L., & Comastri, A. 1998, *MNRAS*, 301, 451, doi: [10.1046/j.1365-8711.1998.02032.x](https://doi.org/10.1046/j.1365-8711.1998.02032.x)
- Giroletti, M., Taylor, G. B., & Giovannini, G. 2005, *ApJ*, 622, 178, doi: [10.1086/427898](https://doi.org/10.1086/427898)
- González-Martín, O., Masegosa, J., Márquez, I., Guainazzi, M., & Jiménez-Bailón, E. 2009, *A&A*, 506, 1107, doi: [10.1051/0004-6361/200912288](https://doi.org/10.1051/0004-6361/200912288)
- Grandi, P., Capetti, A., & Baldi, R. D. 2016, *MNRAS*, 457, 2, doi: [10.1093/mnras/stv2846](https://doi.org/10.1093/mnras/stv2846)
- H. E. S. S. Collaboration, Abramowski, A., Aharonian, F., et al. 2015, *A&A*, 577, A131, doi: [10.1051/0004-6361/201525699](https://doi.org/10.1051/0004-6361/201525699)
- Harvey, M., Rulten, C., & Chadwick, P. 2022a, in 37th International Cosmic Ray Conference, 621, doi: [10.22323/1.395.0621](https://doi.org/10.22323/1.395.0621)
- Harvey, M., Rulten, C. B., & Chadwick, P. M. 2022b, *MNRAS*, 512, 1141, doi: [10.1093/mnras/stac375](https://doi.org/10.1093/mnras/stac375)
- Heckman, T. M. 1980, *A&A*, 87, 152
- Hu, X.-K., Yu, Y.-W., Zhang, J., et al. 2024, arXiv e-prints, arXiv:2402.11949, doi: [10.48550/arXiv.2402.11949](https://doi.org/10.48550/arXiv.2402.11949)
- Kalberla, P. M. W., Burton, W. B., Hartmann, D., et al. 2005, *A&A*, 440, 775, doi: [10.1051/0004-6361:20041864](https://doi.org/10.1051/0004-6361:20041864)
- Kantzas, D., Markoff, S., Lucchini, M., et al. 2022, *MNRAS*, 510, 5187, doi: [10.1093/mnras/stac004](https://doi.org/10.1093/mnras/stac004)
- Kiehlmann, S., Lister, M. L., Readhead, A. C. S., et al. 2024, *ApJ*, 961, 240, doi: [10.3847/1538-4357/ad0c56](https://doi.org/10.3847/1538-4357/ad0c56)
- Kneiske, T., & Raue, M. 2010, in 38th COSPAR Scientific Assembly, Vol. 38, 3

- Lanzetta, K. M., Turnshek, D. A., & Sandoval, J. 1993, *ApJS*, 84, 109, doi: [10.1086/191749](https://doi.org/10.1086/191749)
- Li, K. L., Kong, A. K. H., Takata, J., et al. 2014, *ApJ*, 797, 111, doi: [10.1088/0004-637X/797/2/111](https://doi.org/10.1088/0004-637X/797/2/111)
- Lister, M. L., Homan, D. C., Kovalev, Y. Y., et al. 2020, *ApJ*, 899, 141, doi: [10.3847/1538-4357/aba18d](https://doi.org/10.3847/1538-4357/aba18d)
- Ma, X.-H., Bi, Y.-J., Cao, Z., et al. 2022, *Chinese Physics C*, 46, 030001, doi: [10.1088/1674-1137/ac3fa6](https://doi.org/10.1088/1674-1137/ac3fa6)
- Mattox, J. R., Bertsch, D. L., Chiang, J., et al. 1996, *ApJ*, 461, 396, doi: [10.1086/177068](https://doi.org/10.1086/177068)
- Migliori, G., Siemiginowska, A., Sobolewska, M., et al. 2016, in *Active Galactic Nuclei 12: A Multi-Messenger Perspective (AGN12)*, 60, doi: [10.5281/zenodo.163821](https://doi.org/10.5281/zenodo.163821)
- Nalewajko, K. 2013, *MNRAS*, 430, 1324, doi: [10.1093/mnras/sts711](https://doi.org/10.1093/mnras/sts711)
- O'Dea, C. P., & Saikia, D. J. 2021, *A&A Rv*, 29, 3, doi: [10.1007/s00159-021-00131-w](https://doi.org/10.1007/s00159-021-00131-w)
- Principe, G., Migliori, G., Johnson, T. J., et al. 2020, *A&A*, 635, A185, doi: [10.1051/0004-6361/201937049](https://doi.org/10.1051/0004-6361/201937049)
- Ravasio, M., Tagliaferri, G., Ghisellini, G., et al. 2002, *A&A*, 383, 763, doi: [10.1051/0004-6361:20011828](https://doi.org/10.1051/0004-6361:20011828)
- Scarpa, R., & Falomo, R. 1997, *A&A*, 325, 109
- Sikora, M., Stawarz, L., & Lasota, J.-P. 2007, *ApJ*, 658, 815, doi: [10.1086/511972](https://doi.org/10.1086/511972)
- Sun, X.-N., Zhang, J., Lin, D.-B., et al. 2015, *ApJ*, 798, 43, doi: [10.1088/0004-637X/798/1/43](https://doi.org/10.1088/0004-637X/798/1/43)
- Tramacere, A., Giommi, P., Perri, M., Verrecchia, F., & Tosti, G. 2009, *A&A*, 501, 879, doi: [10.1051/0004-6361/200810865](https://doi.org/10.1051/0004-6361/200810865)
- Tramacere, A., Massaro, E., & Taylor, A. M. 2011, *ApJ*, 739, 66, doi: [10.1088/0004-637X/739/2/66](https://doi.org/10.1088/0004-637X/739/2/66)
- Urry, C. M., & Padovani, P. 1995, *PASP*, 107, 803, doi: [10.1086/133630](https://doi.org/10.1086/133630)
- Véron-Cetty, M. P., & Véron, P. 2003, *A&A*, 412, 399, doi: [10.1051/0004-6361:20034225](https://doi.org/10.1051/0004-6361:20034225)
- Wang, X.-Y., Bi, X.-J., Cao, Z., et al. 2022, *Chinese Physics C*, 46, 030003, doi: [10.1088/1674-1137/ac3fa9](https://doi.org/10.1088/1674-1137/ac3fa9)
- Xie, G. Z., Li, K. H., Bai, J. M., et al. 2001, *ApJ*, 548, 200, doi: [10.1086/318670](https://doi.org/10.1086/318670)
- Xing, Y., & Wang, Z. 2015, *ApJ*, 808, 17, doi: [10.1088/0004-637X/808/1/17](https://doi.org/10.1088/0004-637X/808/1/17)
- Xing, Y., Wang, Z.-X., & Takata, J. 2018, *Research in Astronomy and Astrophysics*, 18, 127, doi: [10.1088/1674-4527/18/10/127](https://doi.org/10.1088/1674-4527/18/10/127)
- Yan, D., Zeng, H., & Zhang, L. 2014, *MNRAS*, 439, 2933, doi: [10.1093/mnras/stu146](https://doi.org/10.1093/mnras/stu146)
- Younes, G., Porquet, D., Sabra, B., et al. 2010, *A&A*, 517, A33, doi: [10.1051/0004-6361/201014371](https://doi.org/10.1051/0004-6361/201014371)
- Yu, Y.-W., Zhang, H.-M., Gan, Y.-Y., et al. 2024, *ApJ*, 965, 163, doi: [10.3847/1538-4357/ad2e07](https://doi.org/10.3847/1538-4357/ad2e07)
- Zhang, J., Liang, E.-W., Zhang, S.-N., & Bai, J. M. 2012, *ApJ*, 752, 157, doi: [10.1088/0004-637X/752/2/157](https://doi.org/10.1088/0004-637X/752/2/157)
- Zhang, J., Zhang, H.-M., Gan, Y.-Y., et al. 2020, *ApJ*, 899, 2, doi: [10.3847/1538-4357/aba2cd](https://doi.org/10.3847/1538-4357/aba2cd)
- Zhang, J., Zhang, S.-N., & Liang, E.-W. 2013, *ApJ*, 767, 8, doi: [10.1088/0004-637X/767/1/8](https://doi.org/10.1088/0004-637X/767/1/8)

Table 1. Observations of Chandra and Swift-XRT and Data Analysis Results for NGC 4278

Obs-date	Obs-ID	Exposure [ks]	$N_{\text{int}}^{\text{H}}$ [10^{20}cm^{-2}]	Γ_{X}	PL norm [$10^{-4} \text{Ph keV}^{-1} \text{cm}^{-2} \text{s}^{-1}$]	kT [keV]	Corr.flux [$10^{-13} \text{erg cm}^{-2} \text{s}^{-1}$]	Refs [*]
2000-04-20	398	1.4						a
2005-02-03	4741	37.5	< 6.78	$2.13^{+0.15}_{-0.13}$	$4.28^{+0.43}_{-0.36}$	0.62 ± 0.04	$18.5^{+1.6}_{-0.3}$	a
2006-03-16	7077	110.3		$2.26^{+0.13}_{-0.10}$	$1.82^{+0.17}_{-0.14}$		$8.21^{+0.79}_{-0.21}$	a
2006-07-25	7078	51.4		$2.34^{+0.13}_{-0.12}$	$4.21^{+0.40}_{-0.31}$		$16.5^{+2.0}_{-0.4}$	a
2006-10-24	7079	105.1		$2.38^{+0.12}_{-0.10}$	$3.76^{+0.31}_{-0.22}$		$15.05^{+1.34}_{-0.35}$	a
2007-04-20	7080	55.8		$2.02^{+0.18}_{-0.18}$	$1.10^{+0.16}_{-0.14}$		$6.0^{+0.8}_{-0.3}$	a
2007-02-20	7081	110.7		$2.12^{+0.13}_{-0.12}$	$1.25^{+0.04}_{-0.11}$		$6.4^{+0.7}_{-0.2}$	a
2010-03-15	11269	81.9	< 2.43	$2.14^{+0.13}_{-0.11}$	$0.35^{+0.04}_{-0.03}$	$0.62^{+0.04}_{-0.05}$	1.86 ± 0.06	b
2010-03-20	12124	25.8	< 11.62	$2.29^{+0.41}_{-0.22}$	$0.33^{+0.12}_{-0.08}$	$0.57^{+0.10}_{-0.16}$	1.66 ± 0.11	b
2021			< 52.7	$1.42^{+0.57}_{-0.55}$	$5.88^{+3.24}_{-2.30}$		$43.60^{+14.17}_{-11.69}$	c

* ‘a’ denotes the Chandra observation results obtained from [Younes et al. \(2010\)](#), while ‘b’ and ‘c’ respectively represent the analysis results of Chandra and Swift-XRT observations conducted in this work.

Table 2. SED Fitting Parameters and Derived Jet Powers of NGC 4278

N_0 [$1/\text{cm}^3$]	p_1^*	p_2^*	γ_{min}^*	γ_b	γ_{max}^*	B [G]	δ^*	R^* [cm]	P_e [erg s^{-1}]	P_B [erg s^{-1}]	P_r [erg s^{-1}]	P_{jet} [erg s^{-1}]
3.5×10^4	2.27	3.8	1	4×10^6	3×10^7	0.015	2.7	6.98×10^{15}	6.97×10^{42}	5.99×10^{38}	5.56×10^{41}	7.52×10^{42}

Note: The parameters marked with an asterisk in the superscript remain fixed during SED modeling.

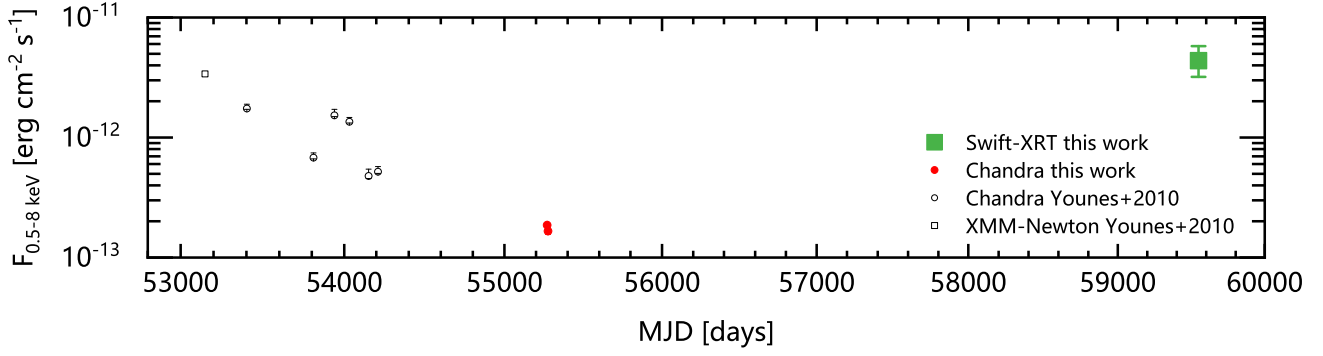


Figure 1. The X-ray light curve of NGC 4278 in the 0.5–8.0 keV band, obtained with the observations from XMM-Newton, Chandra, and Swift-XRT. The data points (black open symbols) before MJD 55000 are directly taken from Younes et al. (2010), while two red circles and one green square represent the analysis results conducted in this work.

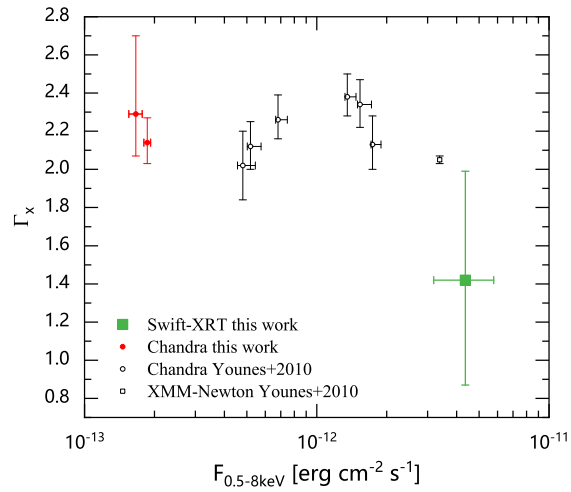


Figure 2. Γ_X vs. $F_{0.5-8 \text{ keV}}$, where the symbols are same as in Figure 1.

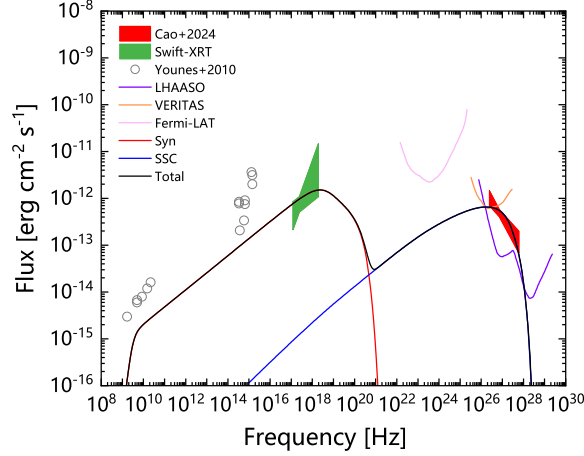


Figure 3. Observed SEDs with model fitting for NGC 4278. The data in radio-optical-UV bands (gray open circles) are taken from [Younes et al. \(2010\)](#). The X-ray spectrum (green bowtie) is derived from the Swift-XRT observations in this work, while the TeV spectrum (red bowtie) is obtained with the LHAASO observations taken from [Cao et al. \(2024\)](#). The black solid line is the sum of each emission component, synchrotron radiation (red line) and SSC process (blue line). The sensitivity curves of LHAASO, VERITAS, and Fermi-LAT are also presented.

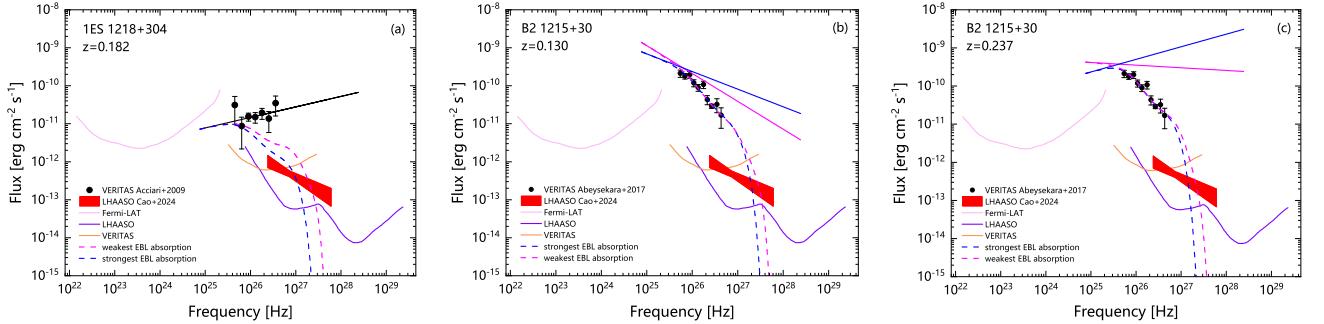


Figure 4. The TeV spectrum of NGC 4278 (red bowtie) is obtained with the LHAASO observations taken from [Cao et al. \(2024\)](#). The blue and magenta dashed lines represent the observable flux level, taking into account the absorption from both the strongest and weakest models of EBL, respectively. The sensitivity curves of LHAASO, VERITAS, and Fermi-LAT are also presented. Panel (a): The intrinsic fluxes (black circles) of IES 1218+304 in the TeV band are taken from [Acciari et al. \(2009\)](#). They are fitted with a power-law function and extrapolated up to the 100 TeV band (black solid line). Panel (b): The observed fluxes of B2 1215+30 in the TeV band are taken from [Abeysekara et al. \(2017\)](#). Considering its redshift of $z = 0.130$, correcting into the intrinsic fluxes with the strongest and weakest models of EBL, fitting them with a power-law function, and extrapolating the fitting lines up to the 100 TeV band, we obtain the blue and magenta solid lines. Panel (c): Same as in Panel (b), but with the redshift of $z = 0.237$.

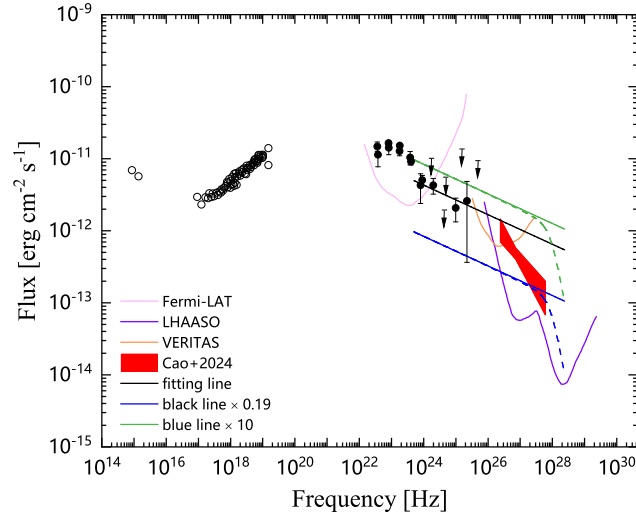


Figure 5. The observed data (black squares, circles, and arrows) of PSR J1023+0038 are taken from [Li et al. \(2014\)](#) and [Xing et al. \(2018\)](#). The black solid line represents the power-law fitting line for the last four detection data points, and it is extrapolated to the 100 TeV band. The blue solid line indicates the possible flux level of the brightest LMXB in MGC 4278, which is obtained by multiplying the black solid line by a factor of 0.19. The green solid line is simply the solid blue line multiplied by 10, assuming that these are several γ -ray emitting LMXBs in NGC 4278. The blue and green dashed lines present the results after considering the EBL absorption.

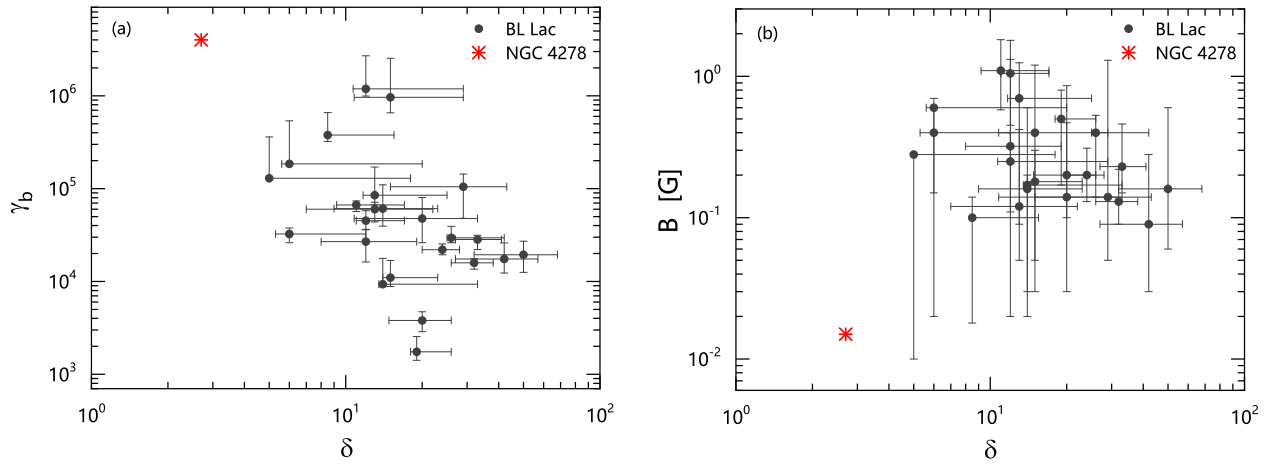


Figure 6. γ_b and B as a function of δ . The data of these typical TeV BL Lacs are from [Zhang et al. \(2012\)](#).

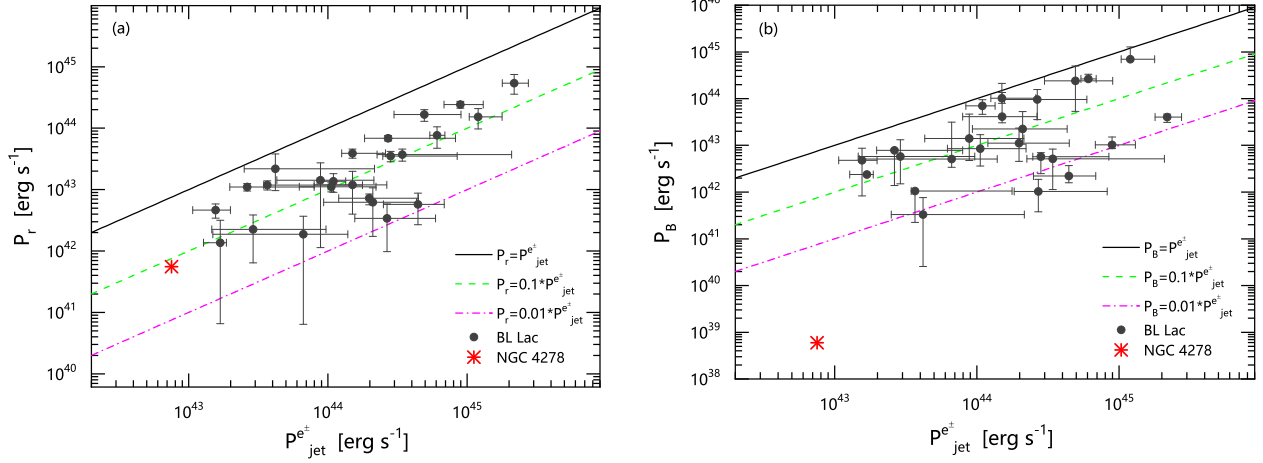


Figure 7. P_r and P_B as a function of $P_{\text{jet}}^{e^\pm}$. The data of these typical TeV BL Lacs are from Zhang et al. (2012).

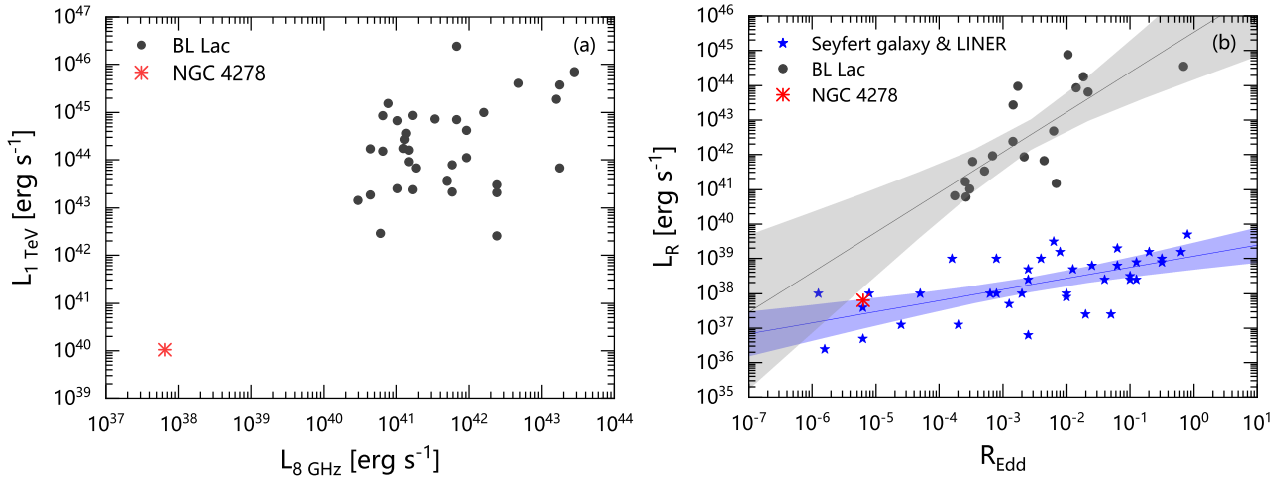


Figure 8. Panel (a): $L_{1 \text{ TeV}}$ vs. $L_{8 \text{ GHz}}$. The data of $L_{8 \text{ GHz}}$ for both NGC 4278 and typical TeV BL Lacs are taken from the RFC, while the $L_{1 \text{ TeV}}$ values of the typical TeV BL Lacs are from Zhang et al. (2012). Panel (b): L_R vs. R_{Edd} , where L_R is the luminosity at 8 GHz for NGC 4278 and BL Lacs taken from the RFC, while it is the luminosity at 5 GHz for seyfert galaxies and LINERs taken from Sikora et al. (2007). R_{Edd} for seyfert galaxies and LINERs is also taken from Sikora et al. (2007), while it is taken from Zhang et al. (2020) for BL Lacs. Note that the BL Lac sample in Panel (b) differs partially from that in Panel (a); for more details, refer to Section 5.3.